ICER-3D: A Progressive Wavelet-Based Compressor for Hyperspectral Images

A. Kiely,[1] M. Klimesh,[1] H. Xie,[1] and N. Aranki[2]

ICER-3D is a progressive, wavelet-based compressor for hyperspectral images. ICER-3D is derived from the ICER image compressor. ICER-3D can provide lossless and lossy compression, and incorporates an error-containment scheme to limit the effects of data loss during transmission. The three-dimensional wavelet decomposition structure used by ICER-3D exploits correlations in all three dimensions of hyperspectral data sets, while facilitating elimination of spectral ringing artifacts. Correlation is further exploited by a context modeler that effectively exploits spectral dependencies in the wavelet-transformed hyperspectral data. Performance results illustrating the benefits of these features are presented.

I. Introduction

Hyperspectral images are three-dimensional (3-D) data sets, where two of the dimensions are spatial and the third is spectral. A hyperspectral image can be regarded as a stack of individual images of the same spatial scene, with each such image representing the scene viewed in a narrow portion of the electromagnetic spectrum. These individual images are referred to as spectral bands. Hyperspectral images typically consist of more than 200 spectral bands; the voluminous amounts of data comprising hyperspectral images make them appealing candidates for data compression.

Exploiting dependencies in all three dimensions of hyperspectral data sets promises substantially more effective compression than two-dimensional (2-D) approaches such as applying conventional image compression to each spectral band independently. With this in mind, we have developed ICER-3D, an extension of the ICER image compressor to hyperspectral images. ICER is a wavelet-based 2-D image compressor; see [1] for a description. ICER is being used onboard the Mars Exploration Rovers for compression of a large majority of the images returned [2]. ICER-3D uses a 3-D wavelet decomposition to provide decorrelation in the spectral dimension as well as both spatial dimensions. Other investigations of 3-D wavelet-based compression of hyperspectral imagery include [3–5].

ICER-3D inherits much of its design, and hence some of its features, from ICER. ICER-3D compression is *progressive*, which means that compressed information is organized so that as more of the

[1] Communications Architectures and Research Section.

[2] Autonomy and Control Section.

The research described in this publication was carried out by the Jet Propulsion Laboratory, California Institute of Technology, under a contract with the National Aeronautics and Space Administration.

compressed data stream is received, reconstructions with successively higher overall image quality can be reproduced. A bitstream with this property is often referred to as *embedded*. ICER-3D uses reversible wavelet transforms, so it can provide lossless or lossy compression. Truncating an embedded data stream by increasing amounts produces a graceful degradation in the reconstructed image quality. Thus, progressive compression provides a simple and effective method of meeting a constraint on compressed data volume.

To limit the effects of data loss during transmission, the wavelet-transformed data are partitioned into a user-selectable number of segments, each roughly corresponding to a rectangular spatial region of the scene. Each segment is compressed independently so that if data pertaining to a segment are lost or corrupted, the other segments are unaffected. Furthermore, because compression is progressive within each segment, when data loss does occur, any received data for the affected segment that precedes the lost portion will allow a lower fidelity reconstruction of that segment.

In Section II we briefly describe the ICER compressor and give an overview of some of the similarities and differences between ICER and ICER-3D. ICER-3D has two key features that distinguish it from a straightforward extension of ICER. First, ICER-3D uses a 3-D wavelet decomposition that includes additional spatial transform stages compared to a 3-D Mallat decomposition; this is described in Section III. Second, ICER-3D uses a bit-plane coding and context modeling procedure that emphasizes spectral (rather than spatial) dependencies in the wavelet-transformed data; this is described in Section IV. In Section V we present performance results that illustrate the benefit to compression effectiveness provided by these two key features. We assume that the reader has a general familiarity with wavelet-based image compression for (2-D) images, and we generally omit the details of ICER-3D compression in areas where it does not differ from ICER.

The examples presented in this article use Airborne Visible/Infrared Imaging Spectrometer (AVIRIS) data [6]. The AVIRIS hyperspectral images referred to in this article have a width of 614 pixels and include 224 spectral bands covering wavelengths from 370 nm to 2500 nm. For most of our examples, we use the first 512-line scene of the calibrated 1997 Moffett Field radiance data set.[3] In this article, we number bands starting from 1 (rather than 0).

II. ICER and ICER-3D

A. ICER Overview

We start with a brief overview of some relevant concepts from the basic (2-D) ICER.

In ICER, multiple stages of a 2-D wavelet transform are applied to the image. The first stage is applied to the whole image, while subsequent stages are applied only to the (horizontally and vertically) low-pass subband from the previous stage. This results in the pyramidal decomposition first suggested by Mallat [7] and currently in common use. The resulting subbands include one small low-pass subband and several subbands that are high-pass in at least one dimension. A three-level 2-D wavelet decomposition of an image is shown in Fig. 1.

ICER's error-containment segments are defined in the transform domain, and each segment approximately corresponds to a rectangular region of the original image. Figure 2 illustrates this correspondence. The partitioning into segments is performed automatically based on the image dimensions and number of segments requested; this operation has no relation to the concept of segmentation for distinguishing objects or regions in an image. Segments are analogous to "precincts" in JPEG2000 [8].

[3] The Moffett Field data set is available from the AVIRIS web site, http://aviris.jpl.nasa.gov.

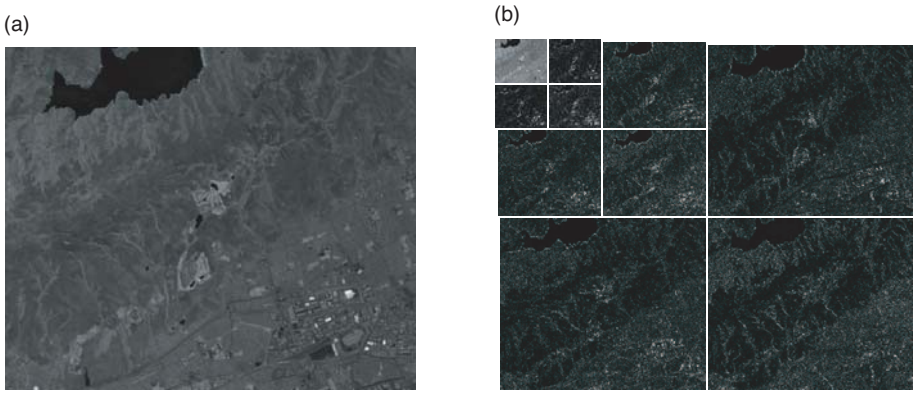

Fig. 1. Example of a three-level, 2-D wavelet decomposition: (a) the original image, spectral band 41 (wavelength 740 nm) from the Moffett Field scene and (b) the result of the wavelet decomposition. In (b), in all subbands except the low-pass subband, absolute values are shown, contrast-enhanced by a factor of 3 relative to the low-pass subband.

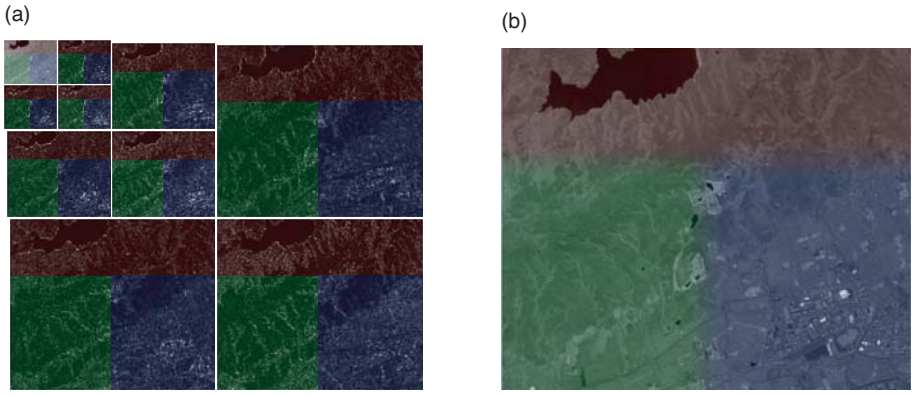

Fig. 2. The image of Fig. 1 divided into three error-containment segments, each tinted a different color: (a) the regions with hard boundaries in the transform domain and (b) the resulting regions with soft boundaries in the original image.

To achieve progressive compression, discrete wavelet transform (DWT) coefficients are converted to sign-magnitude form and encoded one bit plane at a time starting with the most-significant magnitude bit plane. (A bit plane is formed by taking the ith most-significant magnitude bit of each coefficient in a subband, for some i.) When the first '1' bit of a coefficient is encoded, the sign bit is encoded immediately afterward. The wavelet decomposition uses a reversible transform, so lossless compression is achieved when all subband bit planes are coded. Correlation between adjacent coefficients in a subband is exploited via predictive coding and context modeling.

B. ICER-3D Overview

We now give an overview of ICER-3D, along with some comparisons to ICER.

As previously mentioned, hyperspectral data have three dimensions, and ICER-3D uses a 3-D wavelet decomposition. Rather than using a 3-D Mallat decomposition, which would be analogous to the 2-D Mallat decomposition used by ICER, a slightly different decomposition structure is used. Following this wavelet decomposition, mean values are subtracted from spatial planes of spatially low-pass

subbands. These steps are described in Section III, and a detailed discussion of the motivation behind this approach is given in [9,10].

Error-containment segments in ICER-3D are defined spatially (in the wavelet transform domain). The wavelet-transformed data are partitioned in much the same way as in ICER, except that in ICER-3D the segments extend through all spectral bands. Error-containment segments in ICER and ICER-3D are defined using the same rectangle partitioning algorithm; it is described in [1, Section V.D].

In ICER-3D, as in ICER, the trade-off between rate and distortion is controlled by two parameters, one that limits the number of compressed bytes produced and another that limits the number of subband bit planes encoded. The correspondence of this latter parameter to the set of bit planes that can be encoded is described in Sections IV.A and IV.B.

Probability estimates used in the encoding process are derived via context modeling. Under context modeling, a bit of a DWT coefficient to be encoded is classified into one of several contexts based on previously encoded data. In ICER-3D, contexts are defined based on two neighboring coefficients in the spectral dimension and no neighboring coefficients in the same spatial plane. This contrasts with the context modeling scheme used by ICER, which makes use of previously encoded information from spatially neighboring coefficients. The ICER-3D context modeler is described in Section IV.C.

III. Three-Dimensional Wavelet Decomposition

A. Decomposition Structure

When using 3-D wavelet transforms for hyperspectral image compression, systematic variations in signal level of different spectral bands can cause the mean values of spatial planes of spatially low-pass subbands to vary widely. Failing to account for this phenomenon can have detrimental effects on image compression, including reduced effectiveness in compressing spatially low-pass subband data and biases in some reconstructed spectral bands ("spectral ringing") [9].

In ICER-3D these effects are mitigated by the choice of the wavelet decomposition structure used, and by subtracting the mean value from each spatial plane of each spatially low-pass subband. This approach virtually eliminates biases in reconstructed spectral bands and provides an improvement in subjective reconstructed image quality. These benefits are described in more detail in [9]. Here we describe the decomposition procedure used in ICER-3D.

In ICER-3D, the subband decomposition is extended from the 3-D Mallat decomposition so that in stages of decomposition after the first, not only is the low-pass subband further decomposed, but spatially low-pass, spectrally high-pass subbands are also further decomposed spatially. An illustration of this subband decomposition is provided in Fig. 3. The decomposition can be alternately described as follows: first, a 2-D Mallat decomposition with the desired number of levels is performed (spatially) on every spectral band. Then, a single level of spectral decomposition is applied across the first-level spatial subbands; a two-level one-dimensional Mallat decomposition is applied spectrally across the second-level spatial subbands; and so on.[4]

This decomposition structure is motivated by the observation that, in a 3-D wavelet decomposition, the spatially low-pass, spectrally high-pass subbands have spatial planes that look qualitatively similar to spatial planes in the low-pass subband (see [9]). This suggests using additional decompositions of the spatially low-pass, spectrally high-pass spatial planes to improve compression effectiveness in the same

[4] This alternate description does not produce exactly the same result, because the integer DWT is not quite linear due to rounding operations. Another consequence of this nonlinearity is that the decoder should perform the inverse transform operation in exactly the reverse order in which the corresponding forward transforms were performed.

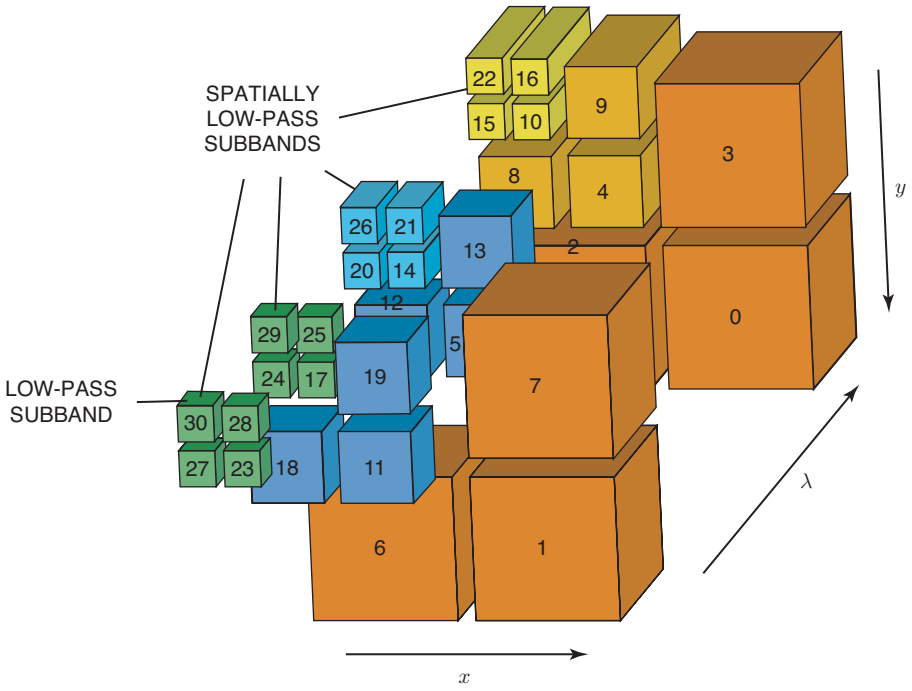

Fig. 3. The 3-D wavelet decomposition scheme used by ICER-3D, illustrated here with three levels of decomposition. The x, y, and λ labels identify the horizontal, vertical, and spectral axes, respectively. Each subband is labeled with an index using the subband numbering scheme described in the Appendix.

way that additional decompositions of the low-pass subband in a 2-D Mallat decomposition improve compression effectiveness.

After the 3-D wavelet decomposition is performed, mean values are computed for and subtracted from each spatial plane of each error-containment segment of each spatially low-pass subband,[5] thus compensating for the fact that such spatial planes often have mean values that are far from zero [9]. The resulting data are converted to sign-magnitude form and compressed (see Section IV). The mean values are encoded in the compressed bitstream and added back to the data at the appropriate decompression step. The overhead incurred by encoding the mean values is only a few bits per spectral band per segment, which is negligible because of the huge size of hyperspectral data sets.

Note that it is important to subtract the means *after* all stages of subband decomposition; otherwise, if two adjacent error-containment segments have significantly different means, a sharp edge would appear after subtracting the means, artificially increasing the high-frequency signal content in further stages of spatial decomposition.

B. Dynamic Range of Wavelet-Transformed Data

In general, the range of possible output values from a reversible DWT can be larger than the range of input values [11]; we refer to such an increase as dynamic range expansion. The amount of dynamic range expansion can increase with multiple filtering operations. Dynamic range expansion can be an issue because storage of wavelet-transformed samples may require binary words that are larger than those used for the original samples. In particular, one must pay attention to the degree of dynamic range expansion

[5] For simplicity of terminology, we use the term "DWT coefficient" to refer to both the coefficient value as well as the value following the mean subtraction operation.

if the wavelet decomposition is performed in-place, i.e., when memory locations originally used to store image samples are subsequently used to store DWT coefficients. Dynamic range expansion is analyzed for ICER in [1]. Here we extend the results to ICER-3D.

For the filters used in ICER and ICER-3D, low-pass filtering does not expand the dynamic range, but high-pass filtering does. The dynamic range expansion following a single one-dimensional high-pass filtering operation can be described (see [1]) by the approximation

$$h_{\max} - h_{\min} \approx (x_{\max} - x_{\min})\gamma$$

Here $x_{\max}$ and $x_{\min}$ denote the maximum and minimum possible values input to the DWT, and $h_{\max}$ and $h_{\min}$ denote the maximum and minimum possible values output from the (one-dimensional) high-pass filtering operation. As noted in [1], $h_{\min} \approx -h_{\max}$. The constant γ is equal to the sum of the absolute values of the filter taps for the linear filter that approximates the particular high-pass filter. Thus, each additional stage of the high-pass filtering operation results in dynamic range expansion by a (filter-dependent) factor γ, or $\log_2 \gamma$ bits. Under the decomposition structure used by ICER-3D, each subband is produced using at most one high-pass filtering operation in each of the three dimensions (x, y, or λ), so the worst-case dynamic range expansion comes from three high-pass filtering operations. Table 1 shows the dynamic range expansion resulting from up to three high-pass filtering operations for the filters used by ICER-3D.

The last column of Table 1 can be used to determine necessary binary word sizes to accommodate dynamic range expansion for a given source bit depth, or conversely, to determine the restriction on source bit depth for a given storage word size. For example, when using filter A, 16-bit words are sufficient to store the coefficients produced by applying a 3-D decomposition to 12-bit data (such as uncalibrated AVIRIS data). But the other filter choices may produce DWT coefficients that cannot be stored in 16-bit words following 3-D wavelet decomposition.

If one is unwilling or unable to provide words of the requisite size for the transform coefficients, there are some possible ways to relax the requirements, with minor costs. For example, quantization of DWT output could be performed at intermediate stages of the decomposition to reduce the dynamic range as needed. This method sacrifices the ability to perform lossless compression, and it may slightly decrease compression effectiveness at high rates, but it may be quite practical when lossless or near-lossless compression is not needed.

Table 1. Approximate dynamic range expansion following one, two, or three high-pass filtering operations.

Filter	One high-pass filter operation		Two high-pass filter operations		Three high-pass filter operations	
	γ	$\log_2 \gamma$, bits	γ^2	$\log_2 \gamma^2$, bits	γ^3	$\log_2 \gamma^3$, bits
A	5/2	1.32	25/4	2.64	125/8	3.97
B	11/4	1.46	121/16	2.92	1331/64	4.38
C	25/8	1.64	625/64	3.29	15625/512	4.93
D	41/16	1.36	1681/256	2.72	68921/4096	4.07
E	47/16	1.55	2209/256	3.11	103823/4096	4.66
F	51/16	1.67	2601/256	3.34	132651/4096	5.02
Q	11/4	1.46	121/16	2.92	1331/64	4.38

For all examples in this article, wavelet transforms are performed using filter A, which is the integer 2/6 DWT filter pair described in [1,12,13].

IV. Bit-Plane Coding

Following the wavelet decomposition and mean subtraction procedure described in Section III.A, each DWT coefficient is converted to sign-magnitude form. Magnitude bit planes of subbands are compressed one at a time; when the first '1' magnitude bit of a coefficient is encoded, the sign bit is encoded immediately afterward. Compressed bit planes of different subbands are interleaved so that earlier bit planes tend to yield larger improvements in reconstructed image quality per compressed bit.

Subband bit planes are compressed in order of decreasing priority value according to the simple priority assignment scheme described below. Bit planes having the same priority value (which are necessarily from different subbands) are compressed in order of decreasing subband index, using the index assignment described in the Appendix.

A. Assigning Priority Values to Subband Bit Planes

For each subband, we can determine a weight that indicates the approximate relative effect, per coefficient of the subband, on mean-squared error (MSE) distortion in the reconstructed image. These weights determine weights of subband bit planes, thereby indicating relative subband bit-plane priorities [1,13]. A subband weight can be expressed in terms of the number of stages of high-pass and low-pass filtering operations, denoted H and L, respectively, used to form a subband. For example, consider subband 21 in Fig. 3. To form this subband, three stages of low-pass filtering are applied in the vertical dimension; two stages of low-pass filtering followed by one stage of high-pass filtering are applied in the horizontal dimension; and one stage each of low-pass filtering and high-pass filtering are applied in the spectral dimension. Thus, $H = 2$ and $L = 6$ for this subband.

The weight w assigned to bit plane b of a subband depends on H and L:

$$w = 2^b \cdot \left(\sqrt{2}\right)^{L-H} = \left(\sqrt{2}\right)^{2b+L-H} \tag{1}$$

Here, bit planes in a subband are indexed starting with $b = 0$ for the least-significant bit. This weight scheme amounts to a 3-D extension of the weight scheme described in [1] for the 2-D case.

Any monotonic function of the weight in Eq. (1) can be used to determine the relative importance of subband bit planes, so rather than keeping track of real-valued weights given by Eq. (1), we define integer "priority" values p of subband bit planes, given by

$$p = 3 + \log_{\sqrt{2}}(w) = 2b + L - H + 3 \tag{2}$$

This definition produces a minimum priority value of 0, since $H \leq 3$ and $L \geq 0$ for all subbands.

As an example, since $H = 2$ and $L = 6$ for subband 21, bit plane b of this subband is assigned priority value

$$p = 2b + 7$$

Thus, all bit planes of subband 21 have odd priority value, with a minimum value of 7. For subband 3, $H = 2$ and $L = 1$, so bit plane b of this subband has priority

$$p = 2b + 2$$

For this subband, all bit planes have even priority value, with a minimum value of 2.

In general, since L and H are fixed for a given subband, all of the bit planes in a subband have even-valued priority, or all have odd-valued priority. As illustrated in Fig. 4, the DWT coefficients with even-valued bit-plane priorities significantly outnumber those with odd-valued priorities.

Additionally, a consequence of the priority definition in Eq. (2) is that only subband 0 has a bit plane with priority 0, and no subbands have bit planes with priority 1. The histogram of Fig. 5 shows the fraction of DWT coefficients that have bits with a given priority value.

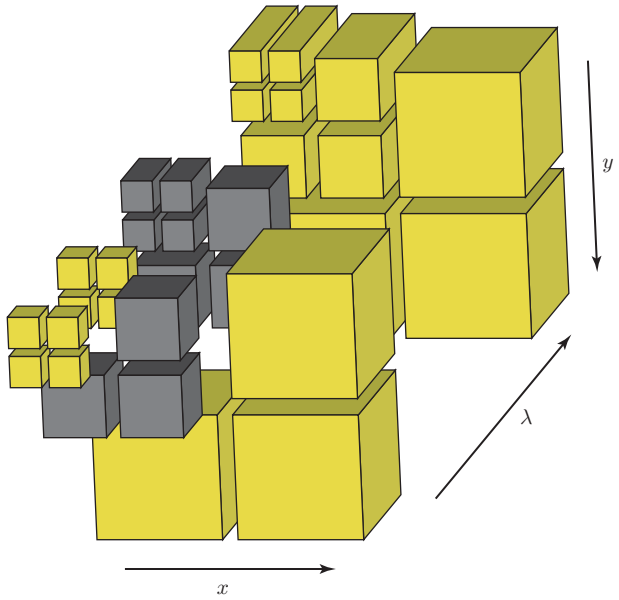

Fig. 4. Bit planes in the dark subbands have only odd-valued priorities. Bit planes in the light subbands have only even-valued priorities.

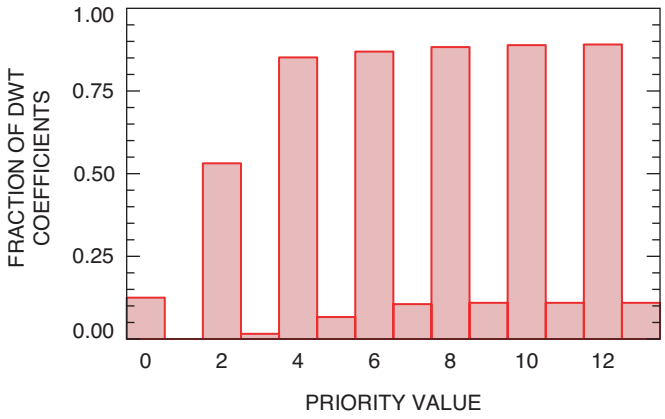

Fig. 5. Fraction of DWT coefficients that have a bit plane with a given priority value for three stages of decomposition.

B. Controlling Image Quality and Amount of Compression

ICER-3D provides two parameters that together are the primary means of controlling image quality and amount of compression: a *byte quota*, indicating a rough maximum number of compressed bytes to produce, and an integer *minimum loss* parameter q that tells the compressor to stop when all subband bit planes having priority value q have been encoded. (Note that a lower value of q corresponds to a higher quality.) ICER-3D stops producing compressed bytes once the quality goal (as expressed by the minimum loss value) or byte quota is met, whichever comes first. Setting the minimum loss parameter to zero will result in compression limited only by the byte quota, and thus compression is lossless when the byte quota is sufficiently large.

This is the same strategy for controlling the compressed data volume and image quality as that used in ICER. In both compressors, the minimum loss parameter controls the minimum amount of quantization performed on the DWT coefficients. Each unit increment corresponds to a set of subband bit planes with the next priority value. In general, a minimum loss value of q in ICER is very roughly equivalent to a minimum loss value of $2q$ in ICER-3D, because successive bit planes of a subband have priority values that differ by 1 in ICER and 2 in ICER-3D. This equivalence is approximate because the coefficients do not have corresponding meanings (2-D versus 3-D decomposition) and the proportions of bits with equivalent priority values do not match.

A consequence of the imbalance between the fraction of bits with even-valued and odd-valued priorities, as described in Section IV.A, is that if we plot rate-distortion points obtained by compressing to each value of the minimum loss parameter, the rate-distortion points cluster in pairs, as illustrated in Fig. 6. This phenomenon does not occur in ICER, where the points are more uniformly spaced.

C. Context Modeling

The general strategy used by ICER-3D for encoding subband bit planes is as follows. Before encoding a bit, the encoder calculates an estimate of the probability that the bit is a zero. This probability-of-zero estimate relies only on previously encoded information from the same segment. The bit and its probability-of-zero estimate are sent to the entropy coder, which compresses the sequence of bits it receives. This

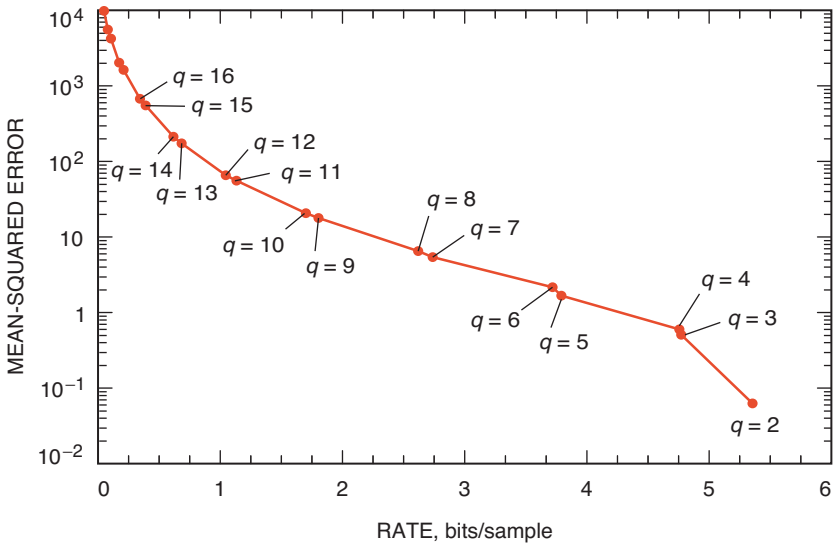

Fig. 6. When compression is limited by the minimum loss parameter q, rate-distortion points cluster in pairs, as illustrated in this example for Moffett Field, scene 1.

strategy is the same as that used by ICER. For entropy coding, ICER-3D uses an interleaved entropy coder; it is the same as that used by ICER, as described in [1, Section IV].

Probability estimates are computed using a technique known as context modeling. With this technique, a bit to be encoded is first classified into one of several contexts based on the values of previously encoded bits. The intent is to define contexts that divide bits with different probability-of-zero statistics into different classes for which separate statistics are gathered. The compressor can then estimate these probabilities of zero reasonably well from the bits it encounters in the contexts. Within this framework, a simple adaptive procedure, also used by ICER and described in [1, Section III.B], is used to estimate probabilities.

ICER-3D employs a one-dimensional spectral context model with context definitions that rely on two neighbors in the spectral direction but no neighbors in the same spatial plane. Note that ICER uses a two-dimensional context model relying on eight (spatial) neighbors.

Encoding of an error-containment segment of a subband bit plane proceeds one spatial plane at a time and in raster scan order within a spatial plane. This encoding order means that a given context will often be assigned many consecutive bits from the same spatial plane, so probability estimation for the context can adapt to the dependency appropriate for the spatial plane being encoded without needing to keep separate statistics for each spatial plane. (For example, when encoding sign bits, the statistics will automatically adapt to exploit both positive and negative correlations between adjacent spatial planes.) In our experiments, maintaining separate context statistics for each spatial plane in a subband segment made little difference in compression effectiveness, but presumably this would not be the case if the coding order were changed.

During the encoding process, ICER-3D maintains a classification of DWT coefficients into *categories*. There are four categories, numbered 0–3. A coefficient's category initially is 0 and remains so as long as the magnitude bits encoded for the coefficient are all zeros; after the first '1' bit from the coefficient is encoded, the coefficient's category becomes 1; when the next magnitude bit from the coefficient is encoded, its category becomes 2; and, finally, when one more magnitude bit from the coefficient is encoded, its category becomes 3 and remains 3 permanently.

ICER-3D uses 19 contexts to classify bits to be encoded that are likely to be compressible. Each context is identified by a label; e.g., we use 1-a through 1-c to identify contexts for bits of DWT coefficients in category 1. Table 2 summarizes the number of contexts used in ICER-3D and ICER for each bit type. The context of a bit is determined using the category of the DWT coefficient containing the bit and the category and signs of the two neighboring coefficients in the spectral dimension. Let C^- and C^+ denote the categories of the neighbors in the previous spatial plane and the next plane, respectively. If one of these coefficients is not available because the coefficient being encoded is in the first or last spatial plane of the subband, the missing coefficients are treated as being in category 0 (i.e., $C^- = 0$ or $C^+ = 0$).

Table 2. Summary of ICER-3D and ICER contexts.

Bit type	ICER-3D	ICER
Category 0	9 contexts	9 contexts
Category 1	3 contexts	2 contexts
Category 2	2 contexts	1 context
Category 3	No compression	No compression
Sign bits	5 contexts	5 contexts
Total	19 contexts	17 contexts

A bit to be encoded from a coefficient in category 0 is classified into one of nine contexts according to Table 3. Further partitioning of contexts based on signs of the spectral neighbors provided no improvement in our experiments. In fact, experiments suggest that contexts 0-g to 0-i (i.e., contexts for which $C^+ \geq 2$) could be sent uncoded without having much impact on compression effectiveness.

Tables 4 and 5 indicate how contexts are assigned to bits of coefficients in categories 1 and 2. We tried further splitting the category 2 contexts based on the value of the preceding bit in the current coefficient, but this made little difference. Bits of coefficients in category 3 are empirically nearly incompressible; that is, estimates of these bits' probabilities of zero tend to be very close to 1/2. Therefore, these bits are left uncoded in the compressor's output.

Sign bits are not encoded directly; rather, the context modeler first predicts the sign bit and then encodes an "agreement" bit that is the exclusive-or of the sign bit and its predicted value. The agreement-bit statistics associated with a sign context are used to estimate a probability of zero for future agreement bits in the context in exactly the same manner as magnitude bits in magnitude contexts.

We use S^- and S^+ to denote the sign bits of the coefficients in the same spatial location in the previous spatial plane and the next plane, respectively, within the subband. We use the symbols $+$, $-$, or 0 to indicate whether the sign bit of the corresponding DWT coefficient is positive, negative, or not yet known. Sign-bit predictions and contexts are assigned according to Table 6.

Table 3. Contexts for bits of DWT coefficients in category 0.

	$C^+ = 0$	$C^+ = 1$	$C^+ \geq 2$
$C^- = 0$	0-a	0-d	0-g
$C^- = 1$	0-b	0-e	0-h
$C^- \geq 2$	0-c	0-f	0-i

Table 4. Contexts for bits of DWT coefficients in category 1.

	$C^+ = 0$	$C^+ = 1$	$C^+ \geq 2$
$C^- < 2$	1-a	1-a	1-a
$C^- \geq 2$	1-a	1-b	1-c

Table 5. Contexts for bits of DWT coefficients in category 2.

	$C^+ < 2$	$C^+ \geq 2$
$C^- < 2$	2-a	2-a
$C^- \geq 2$	2-a	2-b

Table 6. Sign predictions and contexts for sign bits.

	$S^+ = +$	$S^+ = 0$	$S^+ = -$
$S^- = +$	+, S-e	+, S-d	+, S-b
$S^- = 0$	+, S-c	+, S-a	−, S-c
$S^- = -$	−, S-b	−, S-d	−, S-e

In our experiments, sign bits in contexts S-a and S-b tend to be nearly incompressible. This is perhaps not surprising; in context S-a the signs of both spectral neighbors are unknown, and in context S-b the signs of the spectral neighbors have conflicting values. It's tempting to further partition sign bits in these contexts based on signs of (spatially) neighboring coefficients, but our experiments along these lines produced no improvement in compression effectiveness.

Because the contexts for the four types of bits that are compressed (category 0, 1, and 2 bits, and sign bits) do not overlap, the compression of each of these types of bits can be assessed independently. We experimented with using some or all of the spatial context models of ICER in place of the spectral context models used by ICER-3D. Figures 7 through 9 illustrate the benefit provided by the spectral models.

Figure 7 illustrates the impact on rate-distortion performance of altering the context model used for sign bits while using the spatial context models for bits of coefficients in categories 0–2. The spectral sign-bit context model (b) is noticeably more effective than the spatial sign-bit context model (a). Curves (c) and (d) were obtained by assuming each sign bit is compressed to 1 bit or 0 bits, respectively. That is, curve (c) is obtainable by including sign bits in the bitstream without compression, and curve (d) is what one would obtain if sign bits could be encoded for free. Thus, curves (c) and (d) are bounds on the range of rate-distortion performance results that one might obtain by only varying the method of encoding sign bits. We note that the spatial context model for sign bits achieves performance only slightly better than

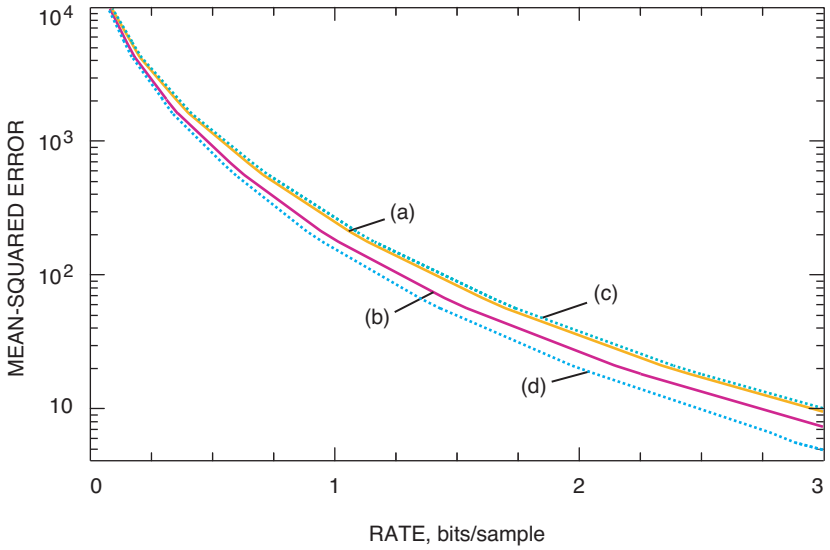

Fig. 7. Rate-distortion results for Moffett Field, scene 1, when sign bits are coded using (a) the spatial context model or (b) the spectral context model. The spatial context models are used for bits of coefficients in categories 0–2. Curves (c) and (d) are bounds obtained by assuming each sign bit is compressed to 1 or 0 bits, respectively.

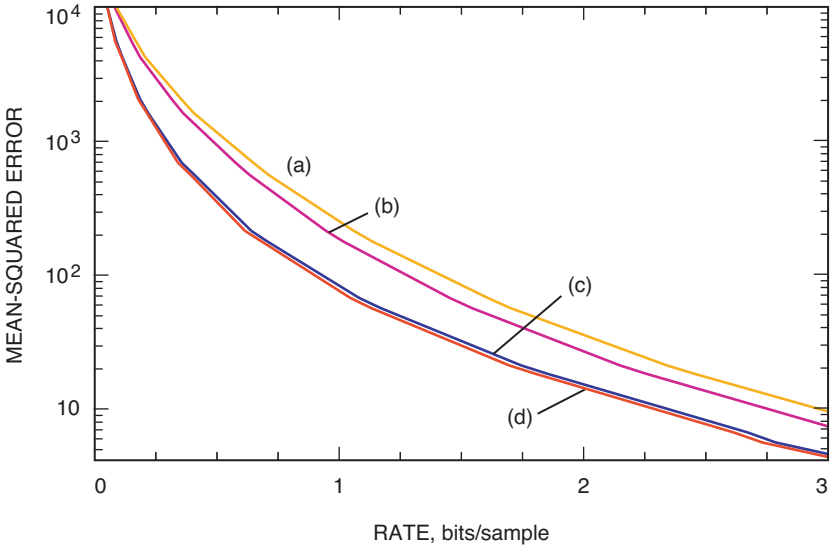

Fig. 8. Rate-distortion results for Moffett Field, scene 1, using (a) the spatial context model for all bits that are compressed; (b) the spatial context model for bits of coefficients in categories 0–2, along with the spectral context model for sign bits; (c) the spatial context model for bits of coefficients in categories 1–2, along with the spectral context model for sign bits and bits of coefficients in category 0; and (d) ICER-3D, which uses spectral context models for all bits that are compressed.

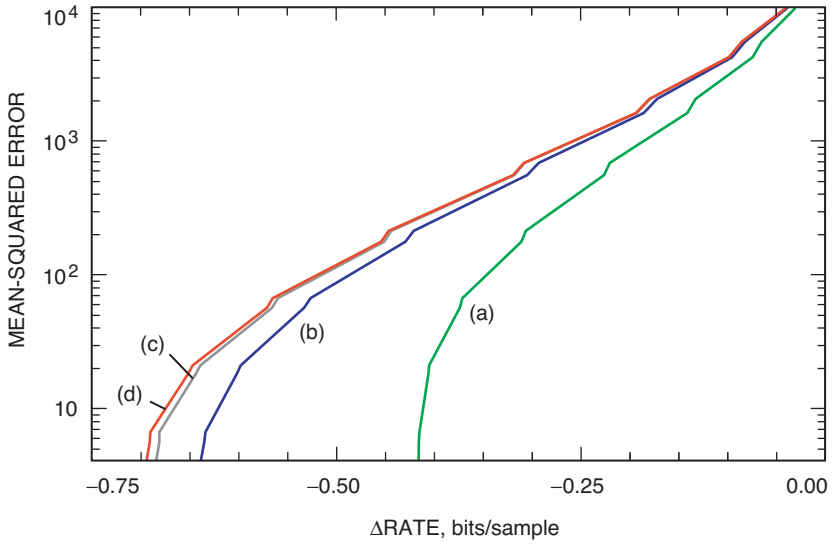

Fig. 9. Difference in bit rate (horizontal axis) versus MSE distortion (vertical axis) achieved by changing from a spatial to a spectral context model for (a) only bits in category 0, (b) bits in category 0 and sign bits, (c) bits in categories 0 and 1 and sign bits, and (d) bits in categories 0–2 and sign bits. Results are shown for Moffett Field, scene 1.

no compression—i.e., sign bits are not well-predicted under the spatial context model. The performance improves noticeably for the spectral context model, suggesting that the spectral context model does a reasonably good job of exploiting strong correlations between adjacent spatial planes of subbands. In our experiments, we observed that the spectral context model for sign bits provides a large improvement over the spatial model for subbands that are spectrally low-pass, and a small improvement in the other subbands.

Figure 8 illustrates the effect on rate-distortion performance as we incrementally convert from a spatial to a spectral context model for the different types of bits that are compressed. Figure 9 illustrates this same effect in terms of the difference in rate achieved. The improvement is significant for sign bits and bits in category 0, and small for bits in categories 1 and 2. In fact, there may be some merit to an implementation in which one sends bits in categories 1 and 2 without compression as a complexity-saving measure; Fig. 10 illustrates the impact that this would have on compression effectiveness. The relatively poor compression performance on bits in categories 1 and 2 is consistent with the conventional wisdom that magnitude bits beyond the first '1' bit in a DWT coefficient are difficult to predict.

V. Results

A. Lossless Compression

Table 7 shows the lossless compression performance of ICER-3D on five 1997 calibrated AVIRIS radiance data sets.[6] For comparison, the table also shows results for the "fast lossless" compressor from [14], the Rice compressor used in the Universal Source Encoder for Space (USES) chip using the multispectral predictor option mentioned in [15], ICER applied independently to individual spatial planes or spatial–spectral planes, and the JPEG-LS image compressor [16] applied independently to individual spatial planes. More extensive lossless hyperspectral compression results for several compressors, including ICER-3D, are available in [14].

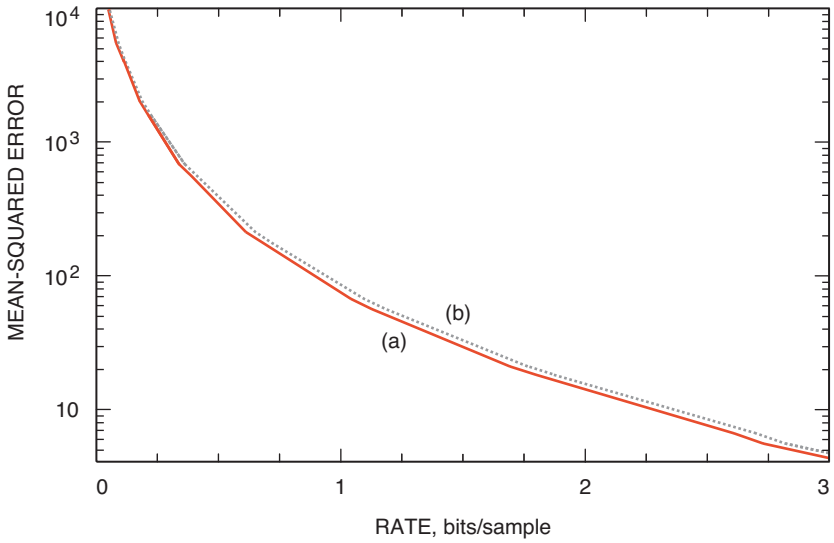

Fig. 10. Rate-distortion results for Moffett Field, scene 1, using (a) ICER-3D (spectral context model for all bits that are compressed) and (b) the spectral context model for sign bits and category 0, but including bits in categories 1 and 2 without compression.

[6] Available from the AVIRIS web site, http://aviris.jpl.nasa.gov.

Table 7. Lossless compression results (rate in bits/sample) for calibrated 1997 AVIRIS radiance datasets. Data for JPEG-LS, Rice/USES, and the "fast lossless" compressor are taken from [14].

Dataset	ICER-3D	Fast lossless	Rice/USES multispectral	ICER spatial–spectral	ICER spatial	JPEG-LS (2-D)
Cuprite	5.21	4.95	6.04	6.13	6.95	7.24
Jasper Ridge	5.42	5.04	6.17	6.24	7.60	7.78
Low altitude	5.63	5.34	6.47	6.41	7.36	7.66
Lunar Lake	5.16	4.97	5.99	6.03	6.79	6.97
Moffett Field	5.33	5.07	6.13	6.11	7.22	7.46
Average	5.35	5.07	6.16	6.18	7.19	7.42

The results of Table 7 indicate that ICER-3D gives more effective lossless compression than simple two-dimensional approaches or the USES multispectral compressor. But ICER-3D is outperformed by the much simpler fast lossless compressor of [14], which would seem to be a preferable compressor when lossless compression is the only concern. However, it could be sensible to use ICER-3D for lossless compression in an application where it is already required to be present to perform lossy compression.

B. Lossy Compression

Figures 11 and 12 show the rate-distortion performance obtained for two AVIRIS scenes. Details from false-color images produced from the reconstructed scenes after compression to 0.1 and 0.25 bits/sample are shown in Figs. 13 and 14, respectively. These images were produced by mapping band 139 to red, 89 to green, and 18 to blue. For all cases, compression was performed using three stages of wavelet decomposition and four error-containment segments.

In each of these figures, result (a) is obtained by applying ICER independently to individual spectral bands, and result (b) is obtained by a straightforward 3-D extension of ICER, specifically, a compressor that uses a 3-D Mallat decomposition and spatial context models. Each result (c) and (d) illustrates the benefit provided by the two key features that distinguish ICER-3D from this straightforward extension: (c) is produced using the modified decomposition and mean subtraction technique combined with the spatial context models, and (d) is obtained when, in addition, the spatial context models are replaced with the spectral models, so that the compressor used is the full ICER-3D.

As an example of the increase in compression effectiveness that can be obtained by exploiting 3-D structure in hyperspectral data, consider the rate-distortion performance shown in Fig. 11 for the Moffett Field scene. To obtain the MSE distortion produced by ICER-3D at 0.25 bits/sample requires about 1.15 bits/sample using ICER applied independently to individual spectral bands, and about 0.55 bits/sample using the 3-D Mallat decomposition combined with the spatial context modeler. Thus, at distortion levels achieved near these rates, a straightforward 3-D extension of ICER yields roughly a factor of 2 reduction in bit rate. ICER-3D attains about an additional factor of 2 reduction in bit rate by using the modified decomposition and mean subtraction combined with the spectral context modeler. Similar results hold for the Cuprite scene, as shown in Fig. 12.

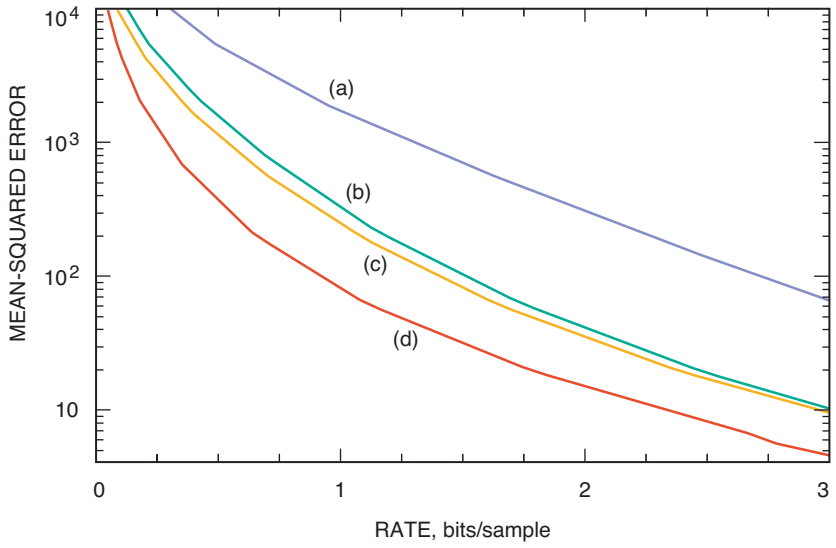

Fig. 11. Rate-distortion results for Moffett Field, scene 1, using (a) ICER applied independently to individual bands, (b) 3-D Mallat decomposition along with the spatial context models, (c) modified decomposition and mean subtraction with spatial context models, and (d) ICER-3D.

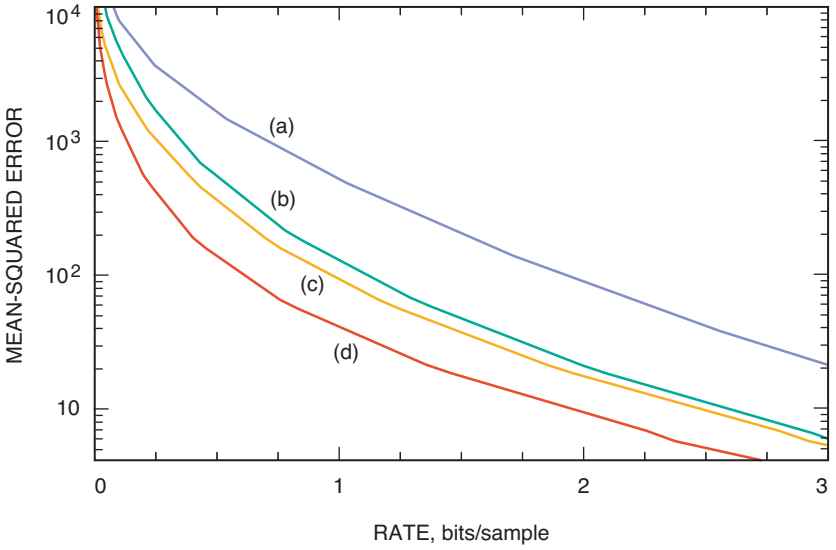

Fig. 12. Rate-distortion results for Cuprite, scene 1, using (a) ICER applied independently to individual bands, (b) 3-D Mallat decomposition along with the spatial context models, (c) modified decomposition and mean subtraction with spatial context models, and (d) ICER-3D.

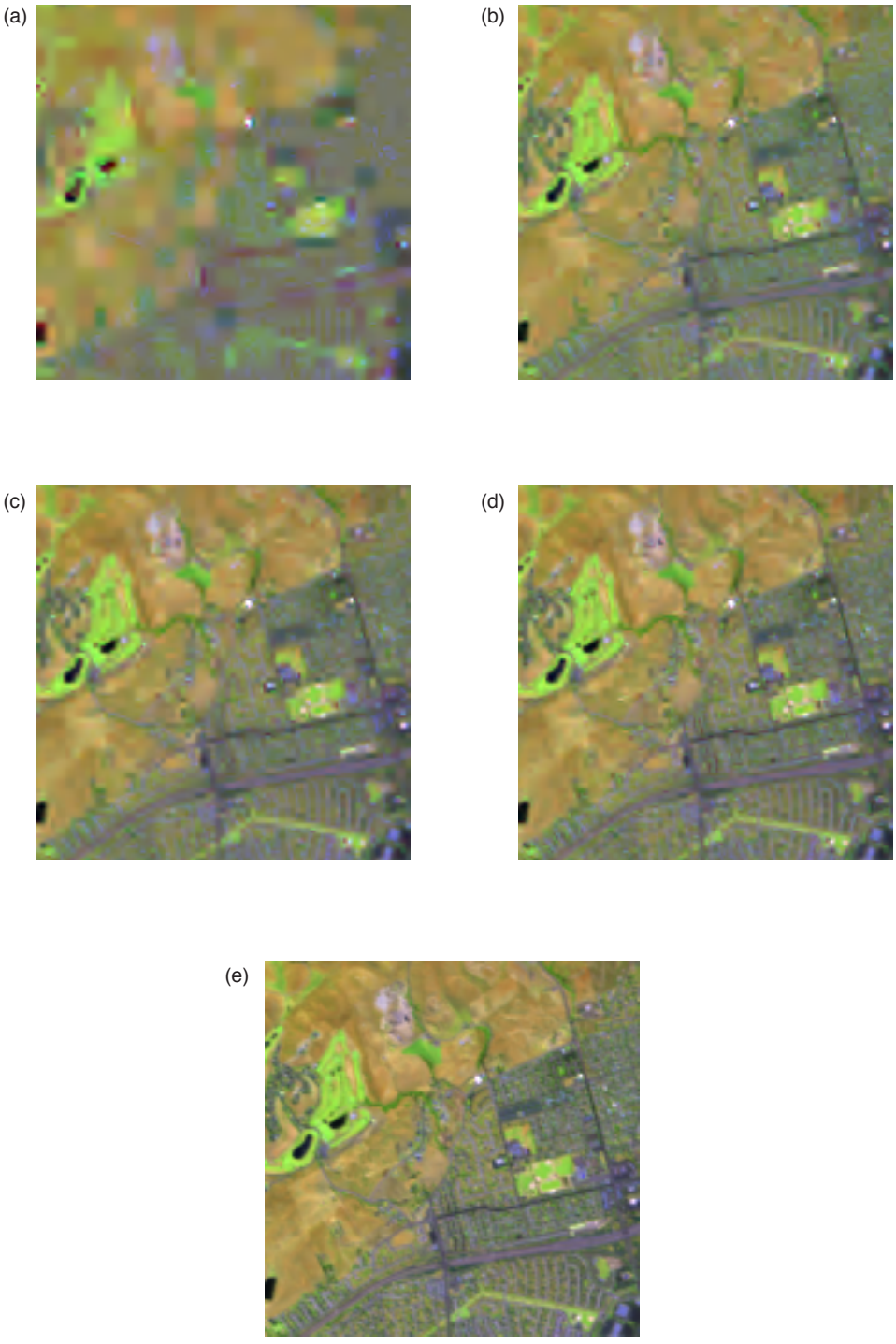

Fig. 13. Details from false-color images produced from the Moffett Field scene compressed using (a) ICER applied independently to individual bands, (b) a 3-D Mallat decomposition combined with the spatial context models, (c) the modified decomposition and mean subtraction technique combined with the spatial context models, and (d) ICER-3D. The original image is shown in (e). In each case, the entire hyperspectral scene was compressed to 0.1 bits/sample.

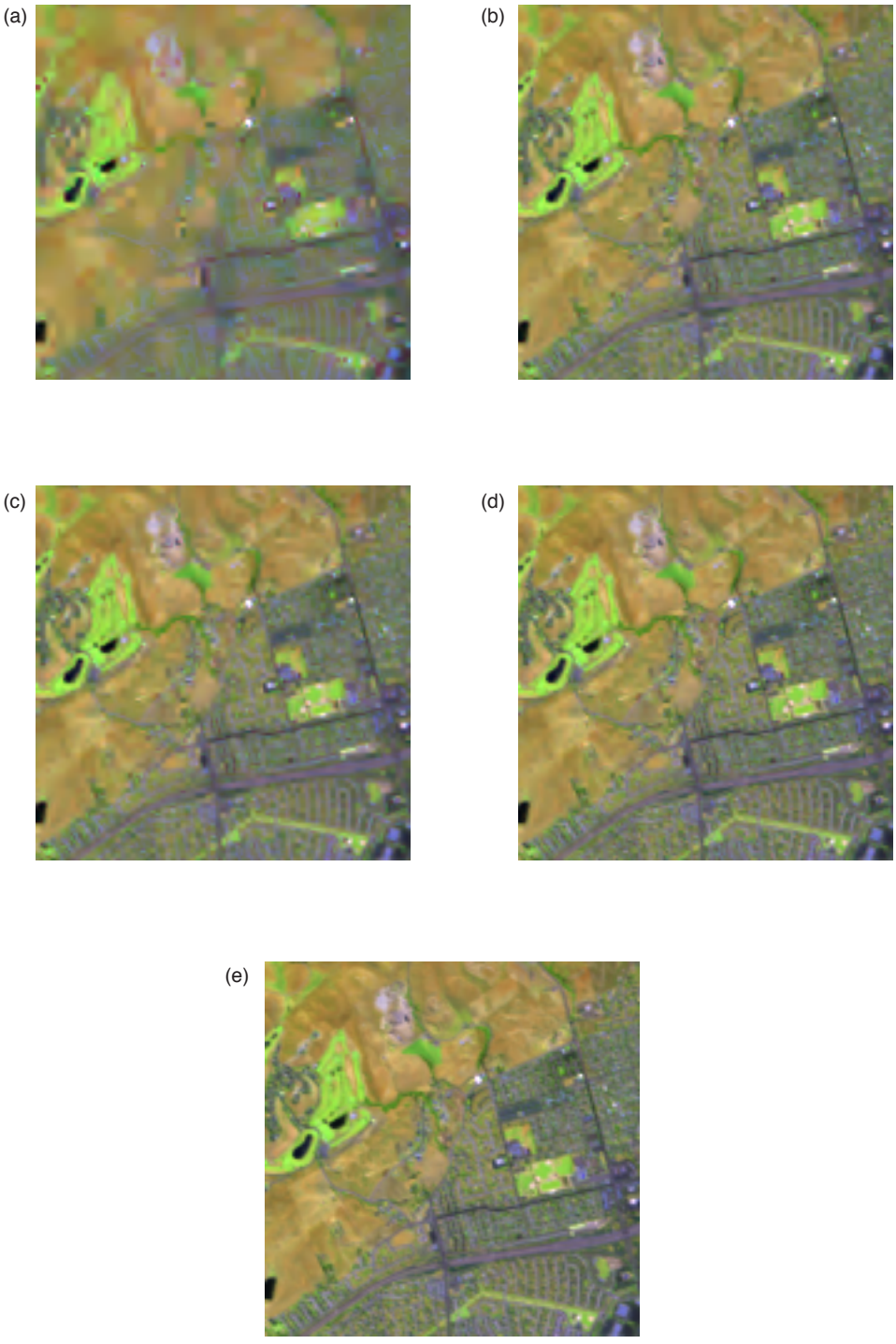

Fig. 14. Details from false-color images produced from the Moffett Field scene compressed using (a) ICER applied independently to individual bands, (b) a 3-D Mallat decomposition combined with the spatial context models, (c) the modified decomposition and mean subtraction technique combined with the spatial context models, and (d) ICER-3D. The original image is shown in (e). In each case, the entire hyperspectral scene was compressed to 0.25 bits/sample.

VI. Hardware Implementation on a Reconfigurable Platform

Given the high data rates produced by hyperspectral imaging instruments and the huge data volumes generated, as well as the fact that ICER-3D is moderately computationally intensive, some missions will find it impractical to use a software implementation of ICER-3D. To address this issue, a hardware implementation has been developed. This effort was led by the fourth author. ICER-3D and the compressor implemented in hardware have some differences that are a result of some of the hardware development predating ICER-3D as described here; we refer to the version implemented in hardware as 'ICER-3D*.'

In ICER-3D* the wavelet decomposition is the three-level Mallat 3-D decomposition, but, as in ICER-3D, mean values are subtracted from each spatial plane of spatially low-pass subbands. The wavelet transform is performed using Filter A. Context modeling is performed using the spatial contexts. A high priority for future work is migration of the new spectral context models to the hardware platform.

The ICER-3D* implementation is on a single Xilinx Virtex II Pro (XC2VP70) field programmable gate array (FPGA) using a commercial board from The Dini Group. The implementation is an encoder that includes efficient implementations of the main modules of ICER-3D*: the 3-D wavelet transform, the context modeler, and the entropy coder. It takes advantage of the embedded PowerPC Reduced Instruction Set Computer (RISC) core and the flexible on-chip bus architecture. The implementation features efficient utilization of off-chip memory through internal buffering to minimize intensive input/output (I/O) operations. The implementation is scalable in that it allows combining of multiple hardware cores in parallel to provide higher throughput. The reconfigurability of the Xilinx Virtex II Pro FPGA allows for the possibility of in situ reprogramming to meet different needs of a single mission without added hardware.

The current prototype provides a throughput of 4.5 Msamples/s for lossless compression with a single module implementation and a conservative clock speed of 50 MHz. The throughput is higher for lossy compression, and would further increase substantially with a higher clock speed and/or use of parallel modules. The power consumption of an implementation with two cores of each module used in parallel is 6.5 W; this implementation utilizes about 60 percent of the chip resources. Further details of the ICER-3D* hardware implementation will be presented in a future article.[7]

VII. Conclusion

The tremendous volume of hyperspectral data sets makes effective data compression an important consideration for any space mission that includes a hyperspectral imager in its payload. Exploiting the 3-D structure of such data sets allows substantially more effective compression than 2-D compression approaches.

ICER-3D exploits 3-D data dependencies in part by using a 3-D wavelet decomposition. The particular decomposition used by ICER-3D includes additional spatial decomposition steps compared to a 3-D Mallat decomposition. This modified decomposition provides benefits in the form of quantitatively improved rate-distortion performance and in the elimination of spectral ringing artifacts.

ICER-3D takes advantage of the correlation properties of wavelet-transformed hyperspectral data by using a context modeling procedure that emphasizes spectral (rather than spatial) dependencies in the wavelet-transformed data. This provides a significant gain over the alternative spatial context modeler considered.

ICER-3D also inherits some important features of ICER, including progressive compression, the ability to perform lossless and lossy compression, and an effective error-containment scheme to limit the effects of data loss on the deep-space channel.

[7] N. Aranki, J. Namkung, and C. Villalpando, "Hyperspectral Data Compression on Reconfigurable Platforms," in preparation for submittal to *The Interplanetary Network Progress Report*.

References

[1] A. Kiely and M. Klimesh, "The ICER Progressive Wavelet Image Compressor," *The Interplanetary Network Progress Report 42-155, July–September 2003*, Jet Propulsion Laboratory, Pasadena, California, pp. 1–46, November 15, 2003. http://ipnpr.jpl.nasa.gov/tmo/progress_report/42-155/156J.pdf

[2] A. Kiely and M. Klimesh, "Preliminary Image Compression Results from the Mars Exploration Rovers," *The Interplanetary Network Progress Report*, vol. 42-156, Jet Propulsion Laboratory, Pasadena, California, pp. 1–8, February 15, 2004. http://ipnpr.jpl.nasa.gov/tmo/progress_report/42-156/156I.pdf

[3] X. Tang, S. Cho, and W. A. Pearlman, "3D Set Partitioning Coding Methods in Hyperspectral Image Compression," *Proc. 2003 International Conference on Image Processing*, vol. II, Barcelona, Spain, pp. II-239–II-242, September 14–17, 2003.

[4] Y. Wang, J. T. Rucker, and J. E. Fowler, "Three-Dimensional Tarp Coding for the Compression of Hyperspectral Images," *IEEE Geoscience and Remote Sensing Letters*, vol. 1, no. 2, pp. 136–140, April 2004.

[5] S. Lim, K. Sohn, and C. Lee, "Compression for Hyperspectral Images Using Three Dimensional Wavelet Transform," *Proc. IEEE 2001 International Geoscience and Remote Sensing Symposium (IGARSS '01)*, vol. 1, Sydney, Australia, pp. 109–111, July 9–13, 2001.

[6] G. Vane, R. Green, T. Chrien, H. Enmark, E. Hansen, and W. Porter, "The Airborne Visible/Infrared Imaging Spectrometer (AVIRIS)," *Remote Sensing of Environment*, vol. 44, pp. 127–143, 1993.

[7] S. G. Mallat, "A Theory for Multiresolution Signal Decomposition: The Wavelet Representation," *IEEE Transactions on Pattern Analysis and Machine Intelligence*, vol. 11, no. 7, pp. 674–693, July 1989.

[8] D. Taubman, "High Performance Scalable Image Compression with EBCOT," *IEEE Transactions on Image Processing*, vol. 9, no. 7, pp. 1158–1170, July 2000.

[9] M. Klimesh, A. Kiely, H. Xie, and N. Aranki, "Spectral Ringing Artifacts in Hyperspectral Image Data Compression," *The Interplanetary Network Progress Report*, vol. 42-160, Jet Propulsion Laboratory, Pasadena, California, pp. 1–17, February 15, 2005. http://ipnpr.jpl.nasa.gov/tmo/progress_report/42-160/160C.pdf

[10] M. Klimesh, A. Kiely, H. Xie, and N. Aranki, "Spectral Ringing Artifacts in Hyperspectral Image Data Compression," *Hyperspectral Data Compression*, G. Motta, F. Rizzo, and J. Storer, eds., New York: Springer, 2006.

[11] B. Masschelein, B. Vanhoof, L. Nachtergaele, J. Bormans, and I. Bolsens, "Implementation Driven Selection of Wavelet Filters for Still Image Coding Based on Bitrange Expansion," *IEEE International Workshop on Multimedia Signal Processing*, Copenhagen, Denmark, pp. 371–376, September 13–15, 1999.

[12] M. D. Adams and F. Kossentini, "Reversible Integer-to-Integer Wavelet Transforms for Image Compression: Performance Evaluation and Analysis," *IEEE Transactions on Image Processing*, vol. 9, no. 7, pp. 1010–1024, June 2000.

[13] A. Said and W. Pearlman, "A New, Fast, and Efficient Image Codec Based on Set Partitioning in Hierarchical Trees," *IEEE Transactions on Circuits and Systems for Video Technology*, vol. 6, no. 3, pp. 243–250, June 1993.

[14] M. Klimesh, "Low-Complexity Lossless Compression of Hyperspecral Imagery via Adaptive Filtering," *The Interplanetary Network Progress Report*, vol. 42-163, Jet Propulsion Laboratory, Pasadena, California, pp. 1–10, November 15, 2005. http://ipnpr.jpl.nasa.gov/tmo/progress_report/42-163/163H.pdf

[15] J. Venbrux, J. Gambles, D. Wiseman, G. Zweigle, W. H. Miller, and P.-S. Yeh, "A VLSI Chip Set Development for Lossless Data Compression," *Ninth AIAA Computing in Aerospace Conference*, San Diego, California, October 19–21, 1993.

[16] M. J. Weinberger, G. Seroussi, and G. Sapiro, "The LOCO-I Lossless Image Compression Algorithm: Principles and Standardization into JPEG-LS," *IEEE Transactions on Image Processing*, vol. 9, no. 8, pp. 1309–1324, August 2000.

Appendix
Subband Index Assignment

Each subband produced by the 3-D wavelet decomposition described in Section III.A is assigned an index, with indices numbered starting from 0. The index assignment is used (along with the bit-plane priority assignment described in Section IV.A) to determine the order in which different subband bit planes are compressed. Figure 3 illustrates the subband indices assigned following three stages of decomposition. In general, indices are assigned by sorting the subbands according to a subband-ordering function, which we now describe.

The subband ordering function is defined by the following rules:

(1) A subband with a larger value of $L - H$ has a higher index. This has the effect of giving higher indices to subbands with higher priority bit planes. (Recall that we denote the number of stages of high-pass and low-pass filtering used to form a subband by H and L, respectively.)

(2) For two subbands with the same value of $L - H$, if one of them has fewer coefficients, then it is given a higher index. (Equivalently, subbands formed through a larger number of wavelet-filtering operations, i.e., larger value of $L + H$, are given a higher index.)

(3) If the two subbands are equivalent in the preceding considerations, then a higher index is given to a subband that is low-pass in the vertical direction.

(4) If the two subbands are equivalent in the preceding considerations, then a higher index is given to a subband that is low-pass in the horizontal direction.

This indexing scheme is somewhat ad hoc, and we have not made much effort to analyze whether another ordering would provide better rate-disortion performance. To first order, bit planes that are assigned the same priority value according to Eq. (2) have approximately the same relative effect, per coefficient of the subband, on MSE distortion in the reconstructed image. Thus, changing the subband indexing scheme isn't likely to have a large impact on rate-distortion performance.